

See discussions, stats, and author profiles for this publication at: <https://www.researchgate.net/publication/259680823>

Reflection Phase and Amplitude Determination of Short-Range Ordered Plasmonic Nanohole Arrays

ARTICLE *in* JOURNAL OF PHYSICAL CHEMISTRY LETTERS · DECEMBER 2013

Impact Factor: 7.46 · DOI: 10.1021/jz402498n

CITATIONS

4

READS

57

2 AUTHORS:



Juliane Junesch

Chalmers University of Technology

9 PUBLICATIONS 111 CITATIONS

[SEE PROFILE](#)



Takumi Sannomiya

Tokyo Institute of Technology

77 PUBLICATIONS 797 CITATIONS

[SEE PROFILE](#)

Reflection Phase and Amplitude Determination of Short-Range Ordered Plasmonic Nanohole Arrays

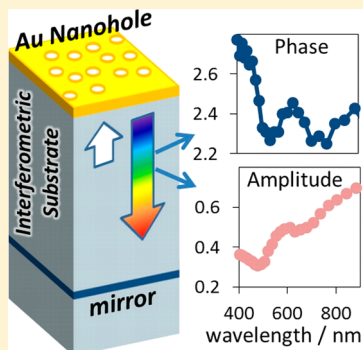
Juliane Junesch[†] and Takumi Sannomiya^{*,‡}

[†]Institute of Biomedical Engineering, ETH Zürich, Gloriastrasse 35, 8092 Zürich, Switzerland

[‡]Department of Metallurgy and Ceramics Science, Tokyo Institute of Technology, 2-12-1, Ookayama, Meguro-ku, Tokyo 152-8552, Japan

Supporting Information

ABSTRACT: The reflection phase and amplitude of a short-range ordered gold plasmonic nanohole array are measured in the vis-NIR range using an interferometric substrate. The phase flip is observed around the minimum of the reflection amplitude, which is consistent with the resonance of a single oscillator. Above the resonance wavelength, the phase shift roughly follows that of a continuous metal film with the same thickness. Numerical simulation of the corresponding hexagonal long-range ordered nanohole array exhibits similar phase behavior with a sharper phase flip at the amplitude minimum, where the field enhancement is strongest. By changing the refractive index of the surrounding medium, larger phase shifts as well as positive and negative amplitude changes were observed around the resonance wavelength. This interferometric substrate method enables simultaneous broad-band phase and amplitude acquisition on the second time scale.



SECTION: Plasmonics, Optical Materials, and Hard Matter

Plasmonic nanohole arrays have been widely investigated for their application as biosensors, chemical sensors, and light-harvesting devices.^{1–5} The plasmonic resonance of the nanohole array originates from the interaction between the nanoholes through surface plasmon polaritons (SPPs).^{6–9} By calculating the SPP wavelength for a given energy, that is, dispersion relation (DR), and adjusting the interhole distance, it is possible to tune the resonance wavelength of the nanohole array.⁹ Recent developments in nanofabrication enabled the production of more complex nanohole devices combined with relatively thick dielectric layers (>100 nm), such as high aspect-ratio nanowells on a niobium oxide layer or nanopores on a supporting silicon nitride membrane.^{10,11} However, these thick dielectric layers introduce optical interference patterns in the spectrum, which disturb the determination of the resonance wavelength for plasmonic sensing. Such interferences are dependent on the refractive index (RI) and the thickness of the dielectric layer as well as the phase shifts and amplitude changes at the two facing interfaces of the dielectric layer.¹² The phase shift caused by the plasmonic nanohole array should be quantified to fully understand and engineer the resonance of such plasmonic nanohole devices on thick dielectrics. However the phase shift by the presence of the nanohole array has scarcely been investigated. In the transmission configuration, it has been reported that the phase shift of a single hole depends on the nanohole diameter, which could be utilized for nanohole lenses.¹³ When the plasmonic devices are integrated into optical circuits, the phase and amplitude determination of the plasmonic structure becomes more important to avoid signal

oscillation or energy loss similar to high-frequency electric devices.

We employ an interferometric substrate to measure the phase and amplitude of the plasmonic nanoholes arranged in a short-range order (SRO). A SRO nanohole array is distinguished from randomly distributed holes by its characteristic interhole distance in the radial direction (Supporting Information). The resonance of the SRO plasmonic nanohole array occurs when the SPP wavelength matches with the characteristic interhole distance.^{9–11} Using interferometric substrates, the phase and amplitude can be easily determined with conventional halogen lamp illumination in a wide wavelength range. So far, phase and amplitude of SRO nanohole arrays have not been studied even for the devices with thick dielectric films, which cause significant interferences and unwanted background in the spectrum. We have previously shown that a long-range ordered (LRO) nanohole array well reproduces the extinction spectrum of the corresponding SRO nanohole array,⁹ yet comparison of the phase is missing. For LRO nanohole arrays, the phase can be obtained from numerical simulation, while the phase of SRO nanohole arrays should be determined experimentally because simulations of SRO arrays require huge calculation spaces and computational loads to obtain reasonable accuracy. Therefore we compare the experimentally acquired phase and amplitude of SRO nanoholes with simulated results of the corresponding LRO

Received: November 19, 2013

Accepted: December 18, 2013

Published: December 18, 2013



structures. The phase measurement also helps to understand the resonance itself because the resonance energy can be uniquely defined as the phase flip by analogy to the resonance of a single oscillator (Supporting Information), while for a nanohole array the conventional intensity spectrum shows a complicated resonance profile with a peak and dip. We also demonstrate dynamic monitoring of the phase and amplitude upon resonance shift by changing RI of the surrounding medium.

Figure 1a shows the schematic illustration of the fabricated SRO gold (Au) nanoholes on top of an etalon structure

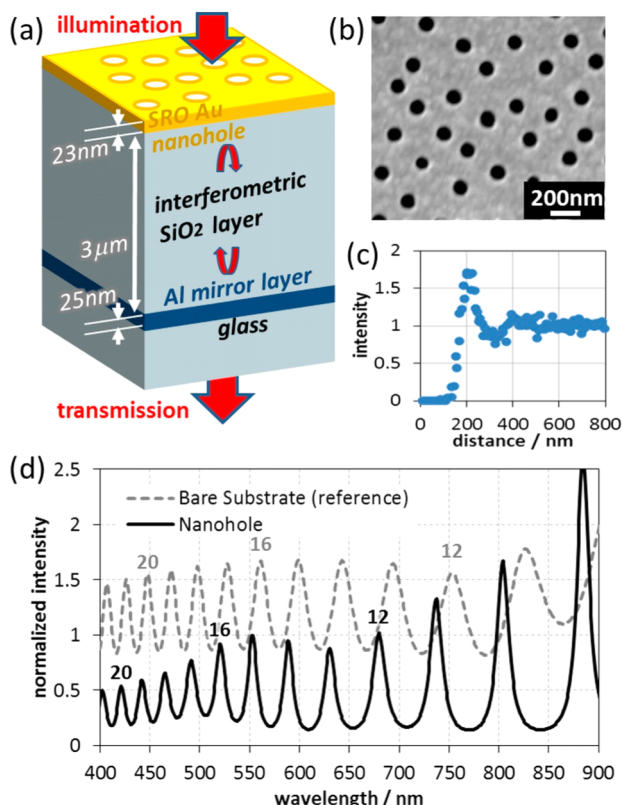


Figure 1. (a) Schematic illustration of short-range ordered (SRO) Au nanoholes on an interferometric substrate. (b) Top-view scanning electron microscopy (SEM) image of the fabricated SRO Au nanoholes. (c) Radial distribution function obtained from the image analysis of a low magnification SEM image. (d) Transmission spectra with (solid line) and without (dashed line) Au nanoholes. The intensity is normalized by the transmission spectrum of a glass substrate with only an Al mirror layer. Chromatic orders m are indicated as numbers on top of some corresponding peaks.

consisting of a 3 μm sputter-coated silicon dioxide (SiO_2) layer and a 25 nm aluminum (Al) reflecting mirror layer on glass.^{14,15} The reflection phase and amplitude at the top interface of the SiO_2 is altered by the presence of the SRO Au nanohole array film. The SRO Au nanoholes with a diameter of 100 nm and thickness of 23 nm were fabricated by colloidal lithography using self-assembled polystyrene colloid masks.^{11,16} Fabrication details can be found in the Supporting Information. The scanning electron microscopy (SEM) image in Figure 1b shows the fabricated SRO 100 nm Au nanoholes. The characteristic center-to-center hole spacing can be estimated from the radial distribution function obtained from SEM image analysis and was found to be ~ 230 nm (Figure 1c). Figure 1d shows the

transmission spectrum of the fabricated sample, illuminated by a collimated halogen lamp. The spectra are normalized by a substrate with only an Al mirror layer to flatten the spectra (compensation of absorption in Al), thus resulting in larger transmission intensities than unity for constructive interferences. For comparison, the spectrum of a bare interferometric substrate is also plotted. The interferometric oscillation amplitudes and peak (dip) wavelengths change by the presence of the nanohole film, corresponding to the changes of the reflection amplitude and phase, respectively.

The exact analysis method to extract the phase and amplitude from the oscillating spectral pattern is described in detail in the Methods section. In short, to obtain the reflection amplitude, we take the intensity ratio of the neighboring peak and dip, which consists of the reflection amplitudes at the facing interfaces of the SiO_2 etalon layer (eq 1). The reflection phase at the top nanohole interface is obtained from the peak (dip) wavelength, considering the chromatic order m and phase shift at the mirror layer interface (eq 2). The absolute amplitude and phase can be determined by comparing them with a control sample without nanoholes, which has the air– SiO_2 interface with known optical properties. We introduced an improved phase determination method because the present nanohole array system has higher background absorption than the previously studied nanoparticle systems and the signal is too noisy to resolve slight changes of the phase and amplitude.¹⁴ The broader dip feature due to the higher reflection amplitude also complicates determination of the dip wavelength position because a slight background tilt results in a large apparent shift of the dip. (See the Methods section.)

The results of the phase and amplitude measurement are shown in Figure 2a,b, together with the theoretically calculated profiles of a continuous 23 nm thick Au film on glass.¹⁷ For the

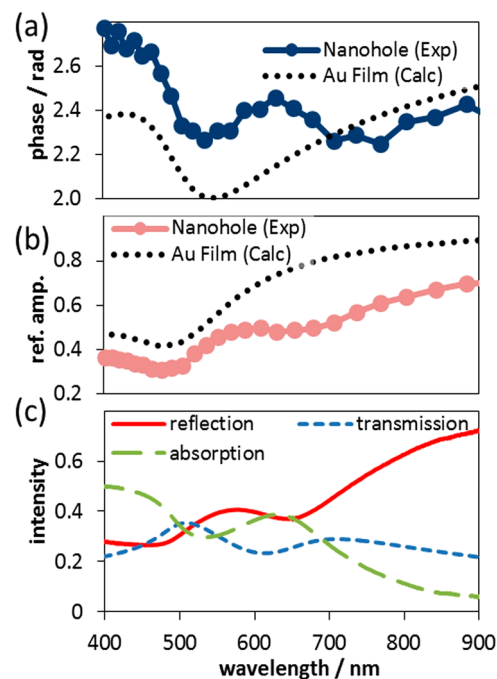


Figure 2. Measured reflection (a) phase and (b) amplitude of the SRO Au nanohole array. For comparison, calculated reflection phase and amplitude of a 23 nm continuous Au film are shown as dotted lines. (c) Reflection, transmission, and absorption spectra of the same nanohole array fabricated on a plain glass substrate.

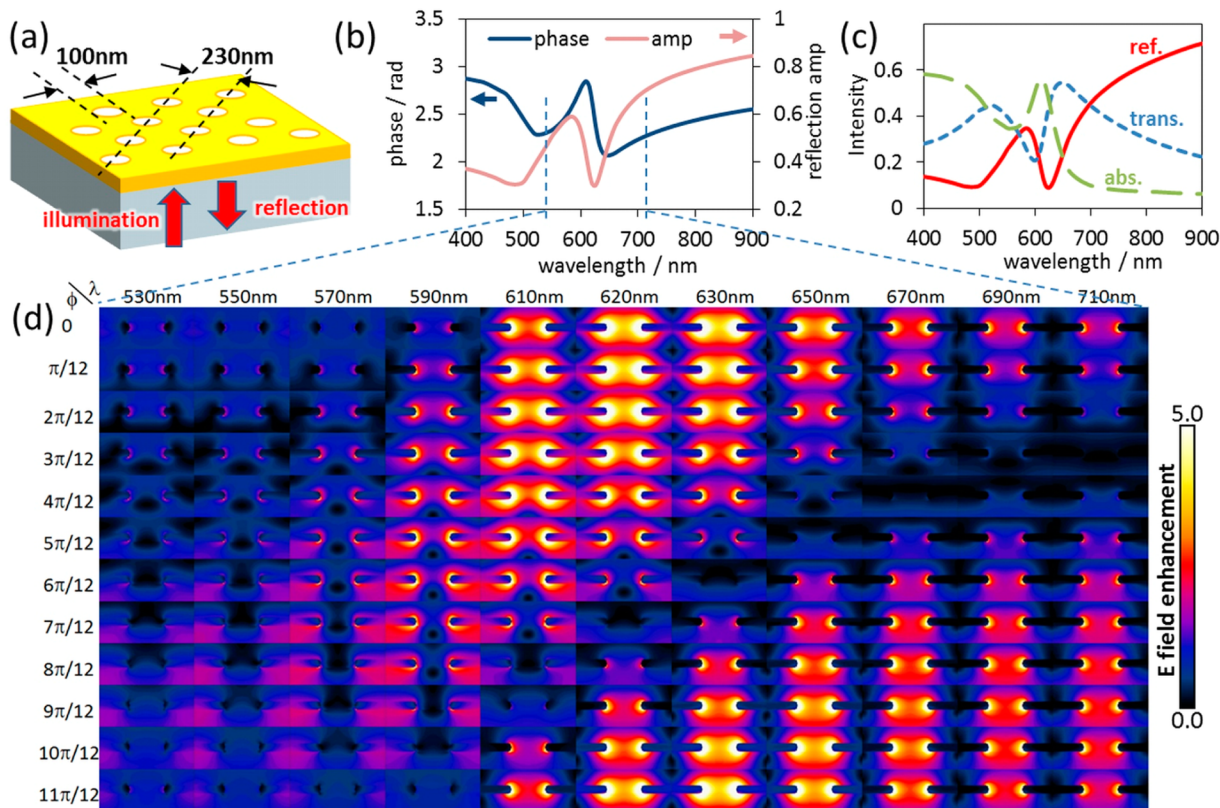


Figure 3. Simulation results. (a) Illustration of the simulated LRO Au nanohole array. (b) Obtained reflection phase and amplitude spectra. (c) Transmission, reflection, and absorption spectra. (d) Phase (phase in vertical axis)-dependent electric field in the wavelength range from 530 to 710 nm (in horizontal axis). The phase zero is fixed as the phase of the illumination plane wave at the center of the hole.

continuous Au film, we use calculated values because the etalon with a continuous Au film on one side and the Al mirror film on the other side gives too-sharp peaks and too-broad dips in the spectrum to determine the phases and amplitudes with enough accuracy. Reasonably smooth curves are obtained for both phase and amplitude of the nanohole array. Above the wavelength of 700 nm, the nanohole phase roughly follows the continuous film, while a clear positive phase difference by ~ 0.4 rad is seen below the wavelength of 700 nm, which is due to the nanohole resonance around 650 nm. The largest phase flip, considering the background of the continuous film, is found at the wavelength of 650 nm, which matches with the minimum of the reflection amplitude. The magnitude of the phase flip is 0.2 to 0.3 rad including the baseline tilt. Because the phase flip generally defines the resonance wavelength^{18,19} (see Supporting Information), the resonance wavelength of the SRO nanohole array should be defined as the reflection minimum, which lies between the transmission (or extinction) maximum and minimum.^{9,19} This shows that the Fano-resonance of the nanohole array, consisting of two “oscillators”, that is, nanoholes and interhole couplings, has a similar phase behavior as the resonance of a single oscillator.^{18,21,22} It also implies that the conventionally used extinction maximum analysis does not exactly correspond to the resonance of a nanohole array. The reflection amplitude of the nanohole array follows the dispersion of the continuous Au film, except for the modulation of the resonance around 650 nm. The amplitude becomes smaller in comparison with the continuous film, especially at the resonance, but gradually approaches the continuous film at longer wavelengths. The magnitude of the measured reflection amplitude at longer wavelengths might be

slightly underestimated because of the inaccurate determination of the intensity of too-sharp oscillation peaks (Figure 1d).

We also compared the reflection amplitude with the intensity spectra by measuring the reflection intensity of nanoholes fabricated on a plain glass substrate illuminated from the glass side. The spectral shape of the measured reflection intensity in Figure 2c is identical to that of the reflection amplitude obtained from the interference spectrum in Figure 2a, which verifies our methodology. The slight quantitative difference most likely originates from the difference of substrate material, namely, sputter-deposited SiO₂ in interferometry and borosilicate glass for simple reflection measurement as well as from the limited coherence and imperfect collimation of the illumination light in the reflection measurement. It should be noted that the intensity is proportional to the square of the amplitude and includes RI at the detection position. Therefore a systematic difference exists between the calculated amplitude from interferometry and the reflection intensity measurement that includes the influence of the glass–air interface. The transmission and absorption spectra are also shown in Figure 2c. The absorption spectrum of SRO nanoholes includes the incoherent light scattering by the nanoholes.

To evaluate and analyze the phase and amplitude of the nanohole array system, we have conducted numerical simulations of LRO Au nanoholes of 100 nm in diameter and 23 nm in thickness in the hexagonal arrangement using a multiple multipole program (MMP). The hexagonal (1 1) interference length was set to 230 nm, which corresponds to the experimental SRO nanohole array. As previously explained, the hexagonal LRO nanohole array well reproduces the extinction maximum wavelength as well as its shift by RI

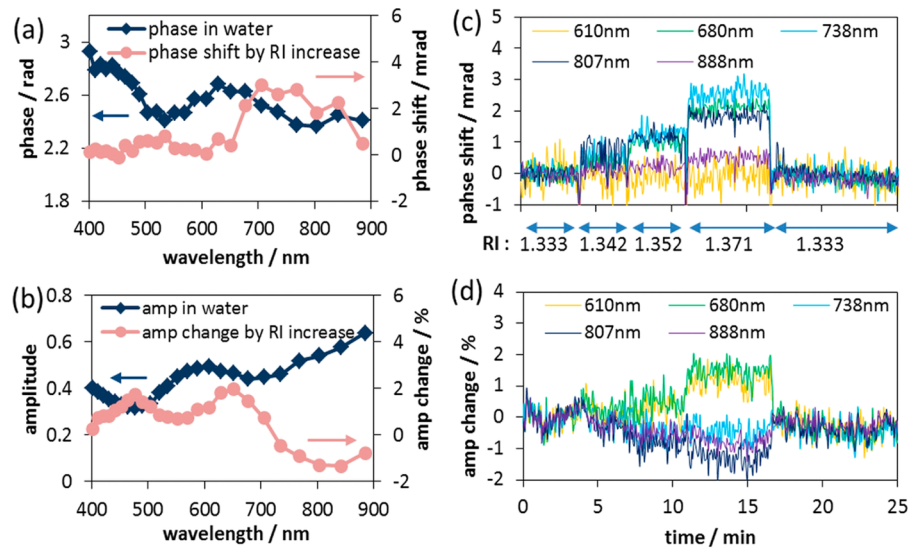


Figure 4. (a) Phase and (b) amplitude spectra in water (dark square) and changes by medium refractive index (RI) change (light circle) from 1.333 in water to 1.371 in 30 wt % glycerol solution. (c) Phase and (d) amplitude responses monitored at different wavelengths while the medium RI was changed, as shown by blue arrows.

changes for sensing.^{9,11} The excitation plane wave was illuminated from the substrate side, and the zero phase (positive maximum of the real field of the incident plane wave) was set at the middle of the hole. The dimension is schematically illustrated in Figure 3a. In the simulation, the reflection phase and amplitude from the substrate side can directly be obtained by comparing the incident and reflection waves. The spectral features of the calculated phase and amplitude in Figure 3b are consistent with the experimental SRO nanoholes, although the resonance of the SRO nanoholes is broader, which is due to the distribution of the interhole distance in SRO. The magnitude of the phase shift relative to the continuous film in Figure 2a is also similar, except for the larger phase flip with sharper inflection around the resonance, of which wavelength corresponds to the amplitude minimum position. The reflection amplitude is smaller for the SRO nanoholes, probably due to the incoherent scattering. The simulated transmission, reflection, and absorption intensity spectra of LRO nanoholes, shown in Figure 3c, agree well with the SRO of Figure 2c, such as relative positions of the peak and dip. For both SRO and LRO, the absorption peak is found between the transmission and reflection minima.

To further investigate the phase at the resonance, we plotted the phase-cross-sectioned electric field of the nanohole by varying the phase and wavelengths around the resonance. The field pattern is summarized in the form of a matrix with horizontal axis in wavelength and vertical axis in phase (Figure 3d). The highest electric field enhancement is found in the wavelength range of 610–630 nm, where the phase of the strongest (weakest) electric field flips over the wavelength. The phase varies only gradually before and after the resonance. The phase-flip wavelengths of the field and the reflection are identical. Thus it can be concluded that the highest field enhancement can be found by the phase-flip wavelength. This is important for applications utilizing field enhancement such as surface enhanced Raman spectroscopy and for RI sensing with location-dependent sensitivity, for example, localized and propagating modes.^{11,23}

Using SRO nanoholes on an interference substrate, we also experimentally investigated how the phase and amplitude of the

nanohole array alter when the resonance shifts due to surrounding RI changes. The sample was first immersed in water (RI 1.333) in a flowcell. The largest phase flip in water occurs around the wavelength of 700 nm, as shown in Figure 4a, indicating the red shift of the resonance compared with the measurement air in Figure 2a. The resonance red shift from air (Figure 2b) to water (Figure 4b) is also found as the shift of the reflection amplitude minimum. To see how the phase and amplitude vary upon a minute resonance shift as well as to verify the possibility of dynamic phase and amplitude observation, we changed the surrounding medium from water to glycerol solution with different concentration while monitoring the spectrum. Figure 4c,d, respectively, shows the phase and amplitude monitored at different wavelengths. With higher RI, high positive phase shifts are observed above the resonant wavelength of 700 nm, while the amplitude plots show negative and positive changes around this resonance wavelength. Milliradian scale changes for the phase shift and few percent changes for the amplitude can be dynamically resolved. The kinetic plots show stable and reproducible responses immediately upon RI increase and decrease, which confirms that solely the bulk RI change was monitored without unstable surface or material property change.^{20,23,24} The wavelength dependence is summarized and superimposed in the spectral plots in Figure 4a,b. The phase shift quickly rises to maximum around the resonance of 700 nm and gradually decays at longer wavelengths. The wavelength range of the positive phase shift is broad, reaching 900 nm, which implies that the resonance in SRO is distributed at the longer wavelengths. This corresponds to the characteristic arrangement of SRO nanoholes with the minimum interhole distance and distribution in longer distances, indicated by the sharp increase in the radial distribution function and the oscillation decay (Figure 1c). It further implies that the SRO structure fabricated by colloidal lithography differs from the SRO array artificially created by displacing certain holes from LRO positions.²⁵ The amplitude change switches the sign from positive below the resonance wavelength to negative at the longer wavelengths. The zero intercept corresponds to the resonance.

This dynamic monitoring technique of two sets of parameters (phase and amplitude) at many different wavelengths may offer the possibility to extract more information of RI changes, for example, location or layer thickness, while conventional plasmonic-sensing techniques have at most three parameters available over the whole wavelengths.^{15,24,26} One simulation example of differentiating the sensing location is shown in the Supporting Information. This technique is also suited for quantitative reflection measurement because the present amplitude measurement is self-referenced by taking the peak-to-dip ratio (PDR, see Methods section) and has least influence of the total intensity change caused for example, by flowcell-air interface or light absorption in the medium. The simplicity and time resolution of this system are advantageous for dynamic and dispersive phase measurement compared with other phase measurement methods, such as Michelson interferometry or two-polarization setups, where a coherent white laser or mechanical phase/polarization adjustment is needed.^{27,28}

In conclusion, we have measured and examined the phase and amplitude of SRO Au nanoholes fabricated on an interferometric substrate using the improved spectral analysis method. The obtained spectrum shows a phase flip corresponding to the wavelength of the reflection amplitude minimum, which should be considered as the resonance wavelength of the Fano-type plasmonic nanohole array as it also coincides with the maximum field enhancement. The resonance shift upon the RI changes accompanied the largest phase shift and the sign flip of the amplitude change around the resonance wavelength. The simulated LRO Au nanoholes with corresponding dimension show consistent phase and amplitude behaviors with the experimental SRO nanoholes except that the spectral modulation of LRO nanoholes is sharper than SRO nanoholes. This understanding of the phase behavior would be the basis to engineer the plasmonic nanohole arrays with thick dielectric layers or to integrate them in optical circuits. For sensing purposes, the thickness and RI of the thick dielectric layer should be designed so that the interference effect does not disturb the plasmonic resonance feature by canceling the phase change of the interference by that of the plasmonic layer, which would result in the flat background in the spectrum. Dynamic monitoring of the phase and amplitude in a wide range of wavelengths may also offer new sensing platforms with more output parameters.

METHODS

To obtain the reflection amplitude ($r_{0(\text{nanohole})}$), we take the peak-to-dip intensity ratio (PDR) of the neighboring peak and dip intensities (I). PDR consists of the reflection amplitudes of the two facing interfaces, namely, at Au nanohole and Al mirror (reflection amplitude: $r_{0(\text{mirror})}$) interface:

$$\begin{aligned} \text{PDR} &= I_{\text{peak}}/I_{\text{dip}} \\ &= 1 + 4r_{0(\text{mirror})} \cdot r_{0(\text{nanohole})}/(1 - r_{0(\text{mirror})} \cdot r_{0(\text{nanohole})})^2 \end{aligned} \quad (1)$$

The phase at the nanohole interface $\Delta\phi_{\text{nanohole}}$ can be calculated from the peak (dip) wavelength because the total phase change by light travel back and forth $\Delta\phi_{\text{total}}$ is $2m\pi$ for the peak and $2(m+1)\pi$ for the dip, where m is the chromatic order (see Figure 1d). Thus, $\Delta\phi_{\text{total}}$ can be expressed as:

$$\begin{aligned} \Delta\phi_{\text{total}}(\lambda) &= 2\pi(2 \cdot n_{\text{etalon}} \cdot L/\lambda) + \Delta\phi_{\text{mirror}}(\lambda) \\ &\quad + \Delta\phi_{\text{nanohole}}(\lambda) \end{aligned} \quad (2)$$

n_{etalon} is the RI of the SiO_2 etalon, L is the etalon length, λ is the wavelength, and $\Delta\phi_{\text{mirror}}$ is the phase shift at the mirror-layer interface. Because the material properties are generally dispersive, the phase shift is a function of the wavelength. Phase and amplitude of the mirror layer can be obtained from the bare substrate without nanoholes because the reflection at the top interface is known. Literature values for the initial optical property of aluminum were used, which were calibrated by measuring a blank sample.²⁹

To exclude the background influence in the determination of the phase, we refined the dip (peak) evaluation procedure by compensating the spectral shift due to absorption. The background spectral inclination was approximated from the neighboring two peaks (dips), and the possible wavelength shift δ due to the background was compensated using the curvature of the peak (dip) C , which has the dimension of $[\lambda^2 T^{-1}]$.

$$\delta_k = [C_k I_k (I_{k+1} - I_{k-1})]/[2(I_{k+1} + I_{k-1})(\lambda_{k+1} - \lambda_{k-1})] \quad (3)$$

Here the suffix k represents the analyzed peak/dip number. To further refine the analysis, we also fitted the dispersive RI of the etalon material by first-order Cauchy's equation so that the chromatic order of the bare substrate sample became an integer over the whole measured wavelength range.²⁰

ASSOCIATED CONTENT

S Supporting Information

Details of methods, resonance of plasmonic nanoholes, simulation of RI sensing, and description of a harmonic oscillator. This material is available free of charge via the Internet at <http://pubs.acs.org>.

AUTHOR INFORMATION

Corresponding Author

*E-mail: sannomiya@mtl.titech.ac.jp.

Notes

The authors declare no competing financial interests.

ACKNOWLEDGMENTS

This work is financially supported by Swiss National Foundation, Iketani Science and Technology Foundation, Japanese Society for the Promotion of Science, and Tokyo Institute of Technology. We thank Prof. J. Vörös from ETH Zurich and Prof. J. Shi from Tokyo Institute of Technology for their advice and discussion.

REFERENCES

- (1) Lal, S.; Link, S.; Halas, N. J. Nano-Optics from Sensing to Waveguiding. *Nat. Photonics* **2007**, *1*, 641–648.
- (2) Jonsson, M.; Dahlin, A. B.; Jönsson, P.; Höök, F. Nanoplasmonic Biosensing with Focus on Short-Range Ordered Nanoholes in Thin Metal Films. *Biointerphases* **2008**, *3*, FD30–FD40.
- (3) Odom, T. W.; Gao, H.; McMahon, J. M.; Henzie, J.; Schatz, G. C. Plasmonic Superlattices: Hierarchical Sub-Wavelength Hole Arrays. *Chem. Phys. Lett.* **2009**, *483*, 187–192.
- (4) Masson, J.-F.; Murray-Methot, M.-P.; Live, L. S. Nanohole Arrays in Chemical Analysis: Manufacturing Methods and Applications. *Analyst* **2010**, *135*, 1483–1489.

- (5) Im, H.; Wittenberg, N. J.; Lesuffleur, A.; Lindquist, N. C.; Oh, S.-H. Membrane Protein Biosensing with Plasmonic Nanopore Arrays and Pore-Spanning Lipid Membranes. *Chem. Sci.* **2010**, *1*, 688–696.
- (6) Ebbesen, T. W.; Lezec, H. J.; Ghaemi, H. F.; Thio, T.; Wolff, P. A. Extraordinary Optical Transmission Through Sub-Wavelength Hole Arrays. *Nature* **1998**, *391*, 667–669.
- (7) Chang, S.-H.; Gray, S. K.; Schatz, G. C. Surface Plasmon Generation and Light Transmission by Isolated Nanoholes and Arrays of Nanoholes in Thin Metal Films. *Opt. Express* **2005**, *13*, 3150–3165.
- (8) Luk'yanchuk, B.; Zheludev, N. I.; Maier, S. A.; Halas, N. J.; Nordlander, P.; Giessen, H.; Chong, C. T. The Fano Resonance in Plasmonic Nanostructures and Metamaterials. *Nat. Mater.* **2010**, *9*, 707–715.
- (9) Sannomiya, T.; Scholder, O.; Jefimovs, K.; Hafner, C.; Dahlin, A. B. Investigation of Plasmon Resonances in Metal Films with Nanohole Arrays for Biosensing Applications. *Small* **2011**, *7*, 1653–1663.
- (10) Jonsson, M. P.; Dahlin, A. B.; Feuz, L.; Petronis, S.; Höök, F. Locally Functionalized Short-Range Ordered Nanoplasmonic Pores for Bioanalytical Sensing. *Anal. Chem.* **2010**, *82*, 2087–2094.
- (11) Junesch, J.; Sannomiya, T.; Dahlin, A. B. Optical Properties of Nanohole Arrays in Metal–Dielectric Double Films Prepared by Mask-on-Metal Colloidal Lithography. *ACS Nano* **2012**, *6*, 10405–10415.
- (12) Born, M.; Wolf, E. *Principles of Optics, Electromagnetic Theory of Propagation, Interference and Diffraction of Light*; Cambridge University Press: New York, 1999.
- (13) Ishii, S.; Shalaev, V. M.; Kildishev, A. V. Holey-Metal Lenses: Sieving Single Modes with Proper Phases. *Nano Lett.* **2012**, *13*, 159–163.
- (14) Sannomiya, T.; Balmer, T. E.; Hafner, C.; Heuberger, M.; Vörös, J. Optical Sensing and Determination of Complex Reflection Coefficients of Plasmonic Structures Using Transmission Interferometric Plasmonic Sensor. *Rev. Sci. Instrum.* **2010**, *81*, 53102–53109.
- (15) Sannomiya, T.; Balmer, T. E.; Heuberger, M.; Vörös, J. Simultaneous Refractive Index and Thickness Measurement with the Transmission Interferometric Adsorption Sensor. *J. Phys. D: Appl. Phys.* **2010**, *43*, 405302.
- (16) Hanarp, P.; Sutherland, D. S.; Gold, J.; Kasemo, B. Control of Nanoparticle Film Structure for Colloidal Lithography. *Colloids Surf, A* **2003**, *214*, 23–36.
- (17) Johnson, P. B.; Christy, R. W. Optical Constants of the Noble Metals. *Phys. Rev. B* **1972**, *6*, 4370–4379.
- (18) Yong, S. J.; Arkady, M. S.; Chang Sub, K. Classical Analogy of Fano Resonances. *Phys. Scr.* **2006**, *74*, 259–266.
- (19) Kedem, O.; Sannomiya, T.; Vaskevich, A.; Rubinstein, I. Oscillatory Behavior of the Long-Range Response of Localized Surface Plasmon Resonance Transducers. *J. Phys. Chem. C* **2012**, *116*, 26865–26873.
- (20) Ikenoya, Y.; Susa, M.; Shi, J.; Nakamura, Y.; Dahlin, A. B.; Sannomiya, T. Optical Resonances in Short-Range Ordered Nanoholes in Ultrathin Aluminum/Aluminum Nitride Multilayers. *J. Phys. Chem. C* **2013**, *117*, 6373–6382.
- (21) Garcia de Abajo, F. J. Colloquium: Light Scattering by Particle and Hole Arrays. *Rev. Mod. Phys.* **2007**, *79*, 1267–1290.
- (22) Lisunova, M.; Norman, J. C.; Blake, P.; Forcherio, G. T.; DeJarnette, D.; Roper, D. K. Modulation of Plasmonic Fano Resonance by the Shape of the Nanoparticles in Ordered Arrays. *J. Phys. D: Appl. Phys.* **2013**, *46*, 485103.
- (23) Schwind, M.; Kasemo, B.; Zorić, I. Localized and Propagating Plasmons in Metal Films with Nanoholes. *Nano Lett.* **2013**, *13*, 1743–1750.
- (24) Dahlin, A. B.; Sannomiya, T.; Zahn, R.; Sotiriou, G. A.; Vöörs, J. Electrochemical Crystallization of Plasmonic Nanostructures. *Nano Lett.* **2011**, *11*, 1337–1343.
- (25) Przybilla, F.; Genet, C.; Ebbesen, T. W. Long vs. Short-Range Orders in Random Subwavelength Hole Arrays. *Opt. Express* **2012**, *20*, 4697–4709.
- (26) Zorić, I.; Zäch, M.; Kasemo, B.; Langhammer, C. Gold, Platinum, and Aluminum Nanodisk Plasmons: Material Independence, Subradiance, and Damping Mechanisms. *ACS Nano* **2011**, *5*, 2535–2546.
- (27) Matsui, T.; Nomura, T.; Miura, A.; Fujikawa, H.; Ikeda, N.; Tsuya, D.; Miyazaki, H. T.; Sugimoto, Y.; Ozaki, M.; Hangyo, M.; Asakawa, K. Wavefront Control by Stacked Metal-Dielectric Hole Array with Variable Hole Shapes. *Opt. Express* **2013**, *21*, 6153–6161.
- (28) Wong, S. L.; Ong, H. C. Phase Difference Mapping of Two-Dimensional Metallic Nanohole Arrays. *Appl. Phys. Lett.* **2012**, *100*, 233102.
- (29) Lide, D. R. *CRC Handbook of Chemistry and Physics*; CRC Press: Boca Raton, FL, 2008.